Acetylcholine nicotinic receptors: finding the putative binding site of allosteric modulators using the “blind docking” approach

Bogdan Iorga, Denyse Herlem, Elvina Barré, Catherine Guillou

Acetylcholine Nicotinic Receptors: Finding the Putative Binding Site of Allosteric Modulators Using the "Blind Docking" Approach

BOGDAN IORGA,* DENYSE HERLEM, ELVINA BARRÉ AND CATHERINE GUILLOU*

Institut de Chimie des Substances Naturelles, CNRS UPR 2301, Avenue de la Terrasse, F-91198 Gif-sur-Yvette, France

e-mail: Bogdan.Iorga@icsn.cnrs-gif.fr; Catherine.Guillou@icsn.cnrs-gif.fr
Tel.: +33 1 69 82 30 30
Fax: +33 1 69 07 72 47

Abstract Allosteric potentiation of acetylcholine nicotinic receptors is considered as one of the most promising approaches for the treatment of the Alzheimer's disease. However, the exact localisation of the allosteric binding site and the potentiation mechanism at the molecular level are presently unknown. We performed the "blind docking" of three known allosteric modulators (galanthamine, codeine and eserine) with the Acetylcholine Binding Protein and models of human $\alpha7$, $\alpha3\beta4$ and $\alpha4\beta2$ nicotinic receptors, created by homology modelling. Three putative binding sites were identified in the channel pore, each one showing different affinities for the ligands. One of these sites is localised opposite to the agonist binding site and is probably implicated in the potentiation process. On the basis of these results, a possible mechanism for the nicotinic acetylcholine receptors (nAChRs) activation is proposed. The present findings may represent an important advance for understanding the allosteric modulation mechanism of nAChRs.

Key words *allosteric modulators acetylcholine nicotinic receptors docking*

Introduction

Alzheimer's disease (AD) [1,2] is the most common form of degenerative dementia of the human central nervous system characterized by progressive memory loss, disorientation, and pathological markers (senile plaques and neurofibrillary tangles). [3] The main existing treatments for AD are the inhibition of acetylcholinesterase (AChE) [4,5] and the blocking of NMDA receptors. [6] Presently, three acetylcholinesterase inhibitors (AChEIs) are available on the market: donepezil (Aricept®), rivastigmine (Exelon®) and galanthamine

(Reminyl®). The memantine (Ebixa®), a NMDA receptors antagonist, is the latest drug released for the treatment of AD.

An interesting alternative for the treatment of AD has emerged in recent years. Indeed, the allosteric modulation of nicotinic acetylcholine receptors (nAChRs) appears as a new, promising approach for the treatment of this disease. [7-17] As the allosteric modulators do not interact with the agonist binding site, the secondary effects due to receptor desensitization observed for the nAChR agonists are expected to be suppressed. [13]

Nicotinic acetylcholine receptors are pentameric membrane proteins traditionally classified into "muscle" and "neuronal" types. The "muscle" nAChRs are heteropentamers with the stoichiometry $(\alpha 1)_2(\beta 1)\gamma\delta$ prior to innervation and $(\alpha 1)_2(\beta 1)\delta\varepsilon$ after innervation. The "neuronal" nAChRs can be classified, based on their subunit composition, in two subtypes: homopentamers consisting of $\alpha 7$–$\alpha 10$ subunits and heteropentamers consisting of various combinations of $\alpha 2$–$\alpha 6$ and $\beta 2$–$\beta 4$ subunits. These subunit combinations confer specific pharmacologies to the nAChRs. [18]

The generally accepted mechanism for the cholinergic neurotransmission implies the binding of ACh to the amino-terminal domains of nAChRs which undergo conformational changes that trigger the opening of the ion channel (gating mechanism). The fixation of an allosteric modulator induces an apparent enhancement of receptor affinity and increases the probability of channel opening. Three different conformations of the nAChRs have been postulated, based on the Monod-Wyman-Changeux model of allosteric transitions: the open, closed and desensitized states. [19] A number of hypotheses concerning the channel opening mechanism have been proposed [20-27] on the basis of the recently published cryo-electron microscopy structures of nAChRs. [28,29] However, the lack of more precise information on the nAChRs three-dimensional structure has limited the attempts to gain molecular insights into the ligand-receptor interaction. The publication of the crystal structure of the Acetylcholine Binding Protein (AChBP), [30-33] a soluble protein homologue to the extracellular domain of nAChRs, bound to HEPES, [30,33] nicotine [33] and carbamylcholine, [33] changed significantly the situation. In functional terms, AChBP shares virtually all of the ligand binding characteristics with the nicotinic receptor family, and reveals a structure largely consistent with the electron microscopy image, chemical

modification, mutagenesis, and spectroscopic data. [34] Considering its sequence identity with the amino-terminal part of α7 nAChR (26%) and the similar behaviour towards the "classical" nAChR ligands, AChBP is considered as a reliable structure for nAChR homology modelling and docking simulations. [35-37] A number of modelled nAChRs structures have been published in recent years. [38-47]

Galanthamine, codeine and eserine (physostigmine) are three known allosteric modulators (allosteric potentiating ligands, APLs) of nAChRs (Figure 1). [9,48-50] Some of them (galanthamine and eserine) show a dual mode of action, being also good AChEIs. This duality confers to galanthamine its effectiveness in the treatment of AD. [5,12,51] In addition, APLs can act as noncompetitive agonists of very low efficacy, and as direct blockers of ACh-activated channels. These actions are observed with nAChRs from brain, muscle and electric tissue. They depend on the structure of the APL and the concentration range applied.[50,52,53]

Place Figure 1 Here

The exact position of the binding site of nAChR APLs is not very clear. [54] Photoaffinity labelling experiments and epitope mapping for the eserine-competitive antibody FK1 have identified the αLys125 residue of *Torpedo* nAChR in the allosteric binding site, or in its immediate vicinity. [55-57] These results have been exploited recently [45] for the docking of eserine in a region defined within 14Å from αLys122 of murine nAChR (corresponding to αLys125 of *Torpedo* nAChR) using the DOCK program. [58]

In this paper we present the results of a more general investigation intending to elucidate the location of the allosteric binding site of nAChRs using the "blind docking" approach, [59] a powerful feature of the AUTODOCK program. [60] For this purpose, we created models of human α7, α3β4 and α4β2 nAChRs on which we docked three allosteric modulators, without imposing a binding site. Three binding sites were identified in the channel pore, one of them being located opposite to the agonist binding site. These findings are discussed and a possible interpretation, considering the experimental results previously published, is proposed.

Materials and methods

Sequence Alignment

The multiple alignment between AChBP and the amino-terminal domains of human α3, α4, α7, β2 and β4 nAChRs subunits was obtained by means of the CLUSTALX package applying the default parameters. [61] The initial alignment was further manually refined.

Model building

The program MODELLER (version 6v2) [62,63] was used to build the three-dimensional models of the amino-terminal domains of human α7, α4β2 and α3β4 nAChRs according to the comparative protein modeling method. The template used was the X-ray structure of AChBP (2.7Å resolution, PDB entry code 1I9B). To maintain the complementarity between subunits at their interfaces, all five units were modeled simultaneously. As expected, the backbone atoms of the predicted models and AChBP overlapped well (RMSD values computed using CHIMERA [64] are 0.71Å for α7, 0.60Å for α3β4 and 0.63Å for α4β2, respectively), due to the algorithm used by MODELLER and to the low number of gaps in the alignment. Additionally, the structures were checked with PROCHECK. [65] The comparison of the Ramachandran plots shows that the models have good quality, with 85–86 % of the residues in the most favourable regions (see Supplementary material). For AChBP and α7 model, the subunit at the clockwise side of each interface as viewed from the *N*-terminus is called "plus" and the other "minus".

Ligand structure

For galanthamine, the coordinates extracted from the X-ray structure of the complex with AChE (PDB entry 1DX6) [66] were used. For codeine and eserine, the coordinates were taken from the Cambridge Structural Database (CSD), entries ZZZTSE01 [67] and ESERIN10, [68] respectively.

Molecular docking

The docking of galanthamine, codeine and eserine into AChBP and human α7, α4β2 and α3β4 models was performed with the program AUTODOCK (version 3.0.5). [60] Its graphical front-end, AUTODOCKTOOLS, [69] was used to add polar hydrogens and partial charges for proteins and ligands using the Kollman United Atom and Gasteiger charges, respectively. Atomic solvation parameters and fragmental volumes for the proteins were assigned using the ADDSOL tool (included in the program package). Flexible torsions in the ligands were assigned with AUTOTORS module and all dihedral angles were allowed to rotate freely. In general, these were all acyclic, non-terminal single bonds (excluding amide bonds) in a given ligand molecule. Affinity grid fields were generated using the auxiliary program AUTOGRID.

The genetic algorithm-local search (GA-LS) hybrid was used to perform an automated molecular docking. Default parameters were used, except for the number of generations, energy evaluations, and docking runs were set to 1,000, 25,000,000 and 256, respectively. The docking process was performed in two steps. In the first one, the docking procedure was realised on the whole protein target, without imposing the binding site ("blind docking"). [59] The grid field was a 60Å cube with grid points separated by 1Å centred at the middle of the protein. In the second step, we docked the ligands in each of the three binding sites found in the first step ("refined docking"). This time, the grid field was a 60Å cube with grid points separated by 0.3Å centred on the best scored conformation obtained in the first step. Lennard-Jones parameters 12–10 and 12–6 (supplied with the program package) were used for modelling H-bonds and Van der Waals interactions, respectively. The resulting docked conformations were clustered into families of similar binding modes, with a root mean squares deviation (RMSD) clustering tolerance of 2Å. In almost all cases the lowest docking energy conformations were included in the largest cluster found (which usually contains 80–100% of total conformations). Otherwise, the lowest docking energy conformations were considered as the most stable orientations. The docking energy represents the sum of the intermolecular energy and the internal energy of the ligand while the free binding energy is the sum of the intermolecular energy and the torsional free energy. [58]

The polar and apolar surface areas of the binding sites were calculated using the GETAREA 1.1 program. [70] The volumes were obtained with the module "SiteID Find Pockets", part of the SYBYL molecular modeling environment, [71] with a 1 Å grid resolution and 3 Å protein film depth, after addition of all hydrogen atoms to the protein. The depth of the binding site was considered as the distance between the most distant spheres generated by the above mentioned module. [71]

Results and discussion

Sequence alignment

Although the sequence identity between the AChBP and the human nAChR extracellular domains is relatively low (18–26 %, Table 1), the presence of highly conserved ACh binding residues in the AChBP [30] and the nicotinic pharmacology of the AChBP [72] suggest that homology modelling of nAChR extracellular domains using the AChBP structure is appropriate.

Place Table 1 Here

The most important requirement in homology modelling is the correct alignment of the sequence to be modelled with that of the template structure. Regions containing insertions relative to AChBP are the greatest sources of uncertainty in modelling. [38] However, only a few insertions are present in our alignment (Figure 2), situated in non-conserved regions, the modelling program used being designed to accommodate them. [73] Several alignments of nAChRs subunits have been previously published, [41-43,45,46] our alignment being very similar to those described by Le Novère et al. [41] The main differences are the residue numbering (our reference is AChBP) and the position of the residues Thr13 and Ala91-Val106, which are shifted one residue lower in our alignment. Henchman et al. [46] used an alignment based on lysine scanning mutagenesis results, involving one supplementary residue of α7 nAChRs at the beginning of the alignment. These differences are observed in regions with low sequence identity, so it is difficult to say which alignment is better.

Place Figure 2 Here

Model building

We used MODELLER [62,63] to generate homology models of extracellular domains of human α7, α3β4 and α4β2 nAChRs using spatial constraints provided by AChBP (see Materials and Methods section). As expected from the model generation algorithm, the output structures do not show major differences with the AChBP structure, as confirmed by the RMSD values for the backbone atoms (0.71Å, 0.60Å and 0.63Å, respectively) and the Ramachandran plots (see Supplementary material). These results are in good accord with those previously reported for the chick α7 model. [41]

Molecular docking

The AUTODOCK program [60] is one of the most reliable docking tools available today, owing its efficiency to the use of a genetic algorithm and to a scoring function comprising several terms (dispersion/repulsion energy, directional hydrogen bonding, screened Coulomb potential electrostatics, a volume-based solvation term, and a weighted sum of torsional degrees of freedom to estimate the entropic cost of binding). [41] Furthermore, it allows the docking of ligands on the entire protein surface, without prior specification of the binding site ("blind docking"). A parameter set based on the AMBER force field [74] and the possibility of using flexible as well as fixed torsions for the ligands during the docking procedure make AUTODOCK an appropriate tool for this purpose. [59] The docking of three known allosteric modulators of nAChRs (galanthamine, codeine and eserine) with AChBP and the models of human α7, α3β4 and α4β2 nAChRs generated before was performed in two steps.

"Blind docking"

In the first step, the "blind docking" approach was used in order to identify the potential fixation sites of nAChRs. The resulting conformations of ligands were clustered (RMSD 2Å) and most of them were found to be located in the channel pore, distributed over three main sites (Figure 3). The first one is located between the L1 and L4 loops (α/+ subunit) and the β3 and β5 sheets (β/– subunit) and the

most important residues are those corresponding to Pro16, Asp17, Leu81, Trp82, Val83, Pro84 and Asp85 (α/+ subunit) and Ser75, Pro77, Pro100 and Leu102 (β/– subunit) of AChBP. The second site is situated between the loops L4 (α/+ subunit) and L5 (β/– subunit), the conserved residues being those corresponding to Val83, Leu86, Ala87, Ala88, Lys94 and Pro95 (α/+ subunit) and Leu98, Thr99 and Pro100 (β/– subunit) of AChBP. The third one is positioned close to the L5 loop and β7 and β2 sheets (β/– subunit) and comprises mainly the residues corresponding to Asp49, Ser93, Lys94, Pro95, Glu96, Arg118, Gln119 and Arg120 (β/– subunit) of AChBP. For more details about the residues composing these three binding sites see Figure 2 and Tables S1-S3.

Place Figure 3 Here

An important finding is the location of the first binding site, situated exactly opposite to the agonist binding site, at less than 12Å through the protein wall. The proximity of these two sites, as well as the high affinity of the ligands for this allosteric site suggest that the allosteric site 1 plays an important role in the potentiation of the nAChR. Indeed, the most direct manner to transmit an information between two sites is to place them nearby. It must be pointed out that for the first crystallographic structure of AChBP [30] all the seven structural water molecules present in the channel pore observed are located in this allosteric site 1. Additionally, it is worth noting that this high affinity binding site was evidenced without imposing any constraint and in the absence of water molecules in the docking process.

Some differences in the population of the three sites were observed (Table S4 in Supplementary material), depending on the nature of protein and ligand, but two remarks can be made: a) in all cases, the great majority of conformers were found in the sites 1 and 2 and b) the docking energy and the free binding energy of the conformations found in the third site were always higher than those found in the sites 1 and 2 (Tables S5 and S6 in Supplementary material). As the lack of flexibility in the protein may influence the binding modes of the ligands and the affinities and orientations may importantly vary from one site to other one, these results should be considered with care. However, the agonist binding site of acetylcholine nicotinic receptors has been correctly identified previously using

AUTODOCK on homology models constructed in a similar manner. [41] The reproducibility observed for all these dockings may suggest that the third site shows an apparent low affinity for the allosteric modulators, in contrast with the sites 1 and 2. Considering the position of this third site at the bottom of the ligand binding domain, it might be also implicated in the modulation of the motions needed for opening/closing the narrow ion gate of the transmembrane domain. Additionally, the third site is situated not far from the location previously identified as the allosteric site by photoaffinity labelling, [55,56] and used later for docking studies. [45] However, the experimental protocol used for the photoaffinity labelling (irradiation of nAChR-enriched *Torpedo marmorata* membrane fragments incubated with 8-azidoATP and [^{3}H]physostigmine) [55,56] allows only the identification of allosteric sites located in close proximity to an ATP binding site. [75-77]

Several parameters of these three allosteric sites identified by "blind docking" have been calculated (polar and apolar surface areas, volume and depth) and compared with those of the agonist binding site (Table S7 in Supplementary material). The sites are mostly hydrophobic, with some polar regions. The site 1 is rather narrow and deep, similar to the agonist site, whereas the sites 2 and 3 are more open and less deep. The third site is smaller than the other ones, and this may explain the weaker affinity of the allosteric ligands observed for this site.

"Refined docking"

In the second step, the ligands were docked in each of the three binding sites previously found ("refined docking"). The use of an improved grid resolution allows a better evaluation of the protein-ligand interactions, and consequently lower docked energies are obtained with respect to the "blind docking" (see Table S5 in Supplementary material). The Figure 4 shows some representative binding modes of the best docked conformations in the three allosteric sites. The hydrogen bonds were automatically identified using the CHIMERA's "FindHBond" module [64] and the other interactions were visually evidenced, with a cut-off distance of 4Å. In most cases, a salt bridge was observed between the positive nitrogen atoms of the ligands and Asp or Glu residues of the protein. Additionally, the oxygen atoms of the ligands were found to be implicated in hydrogen bonds and electrostatic interactions with the protein residues.

Place Figure 4 Here

On the basis of the results presented above, a possible mechanism for the allosteric activation of the nAChRs can be outlined. We propose the existence of three allosteric binding sites showing different affinities for the allosteric modulators. Since the reversibility of the allosteric modulators binding is generally accepted [53] we can presume an exchange of the ligands between the three allosteric sites. The allosteric binding in the first site probably induces an increase of the agonist binding affinity as a consequence of the proximity of these two sites, which might be connected through a hydrogen bond network in which protein residues and structural water molecules are involved. On the other hand, despite its apparent low affinity for the ligands, the third site may be implicated the transmission of the allosteric deformation from the agonist site to the transmembrane domain, due to its key position at the interface between the transmembrane and ligand binding domains. All these processes will result in an increase of gate opening frequency and the overall potentiation of nAChRs. Additional work is in progress in our laboratory to obtain more information about the exact nature of the interaction between the two adjacent sites, especially the role of the structural water molecules in the activation process. The validation of these results by means of photoaffinity labelling and mutagenesis studies is under way and will be presented elsewhere.

Conclusions

In the present work we generated models of human α7, α4β2 and α3β4 nAChRs by homology modelling, which were docked with three known allosteric modulators of nAChRs using the "blind docking" approach. Three binding sites were identified in the channel pore, one of them being situated in the immediate proximity of the agonist binding site. We propose a possible mechanism for the nAChRs activation, which is the first attempt to rationalise this process at the molecular level. Further studies are in progress to investigate the role of crystallographic water molecules in the activation, probably through a hydrogen bond network. The identification of the allosteric binding site(s) of the nAChRs

will subsequently allow the design of new molecules for the treatment of Alzheimer's disease.

Acknowledgements We thank to the Centre National de la Recherche Scientifique (CNRS) for the financial support.

Supplementary material available Ramachandran plots of the models created by homology, representative binding modes of the most stable docked orientations found (Figures S1-S2), list of residues of the three binding sites (Tables S1-S3), distribution of populations on the three binding sites and estimated docking energies in "blind docking" (Table S4), estimated docking energies (Table S5) and free binding energies (Table S6) in "refined docking", parameters of the allosteric sites identified by "blind docking" compared with those of the agonist site (Table S7).

References

1. Alzheimer A (1906) Neurolisches Zentralblatt 25: 1134
2. Möller HJ, Graeber MB (1998) Eur Arch Psychiatry Clin Neurosci 248: 111-122
3. Mattson MP (2004) Nature 430: 631-639
4. Lane RM, Kivipelto M, Greig NH (2004) Clin Neuropharmacol 27: 141-149
5. Ibach B, Haen E (2004) Curr Pharm Des 10: 231-251
6. Rogawski MA, Wenk GL (2003) CNS Drug Rev 9: 275-308
7. Maelicke A, Schrattenholz A, Samochocki M, Radina M, Albuquerque EX (2000) Behav Brain Res 113: 199-206
8. Maelicke A (2000) Dement Geriatr Cogn Disord 11 Suppl. 1: 11-18
9. Maelicke A, Albuquerque EX (2000) Eur J Pharmacol 393: 165-170
10. Changeux J, Edelstein SJ (2001) Curr Opin Neurobiol 11: 369-377
11. Pereira EF, Hilmas C, Santos MD, Alkondon M, Maelicke A, Albuquerque EX (2002) J Neurobiol 53: 479-500
12. Woodruff-Pak DS, Lander C, Geerts H (2002) CNS Drug Rev 8: 405-426
13. Geerts H, Finkel L, Carr R, Spiros A (2002) J Neural Transm Suppl: 203-216
14. Bourin M, Ripoll N, Dailly E (2003) Curr Med Res Opin 19: 169-177
15. Doggrell SA, Evans S (2003) Expert Opin Investig Drugs 12: 1633-1654
16. Romanelli MN, Gualtieri F (2003) Med Res Rev 23: 393-426
17. Hogg RC, Bertrand D (2004) Curr Drug Targets CNS Neurol Disord 3: 123-130
18. Maelicke A, Schrattenholz A, Albuquerque EX (2000) In: Clementi F, Fornasari D, Gotti C (eds) Neuronal nicotinic receptors. Springer, Berlin pp 477-496
19. Edelstein SJ, Schaad O, Henry E, Bertrand D, Changeux JP (1996) Biol Cybern 75: 361-379
20. Unwin N, Miyazawa A, Li J, Fujiyoshi Y (2002) J Mol Biol 319: 1165-1176
21. Unwin N (2003) FEBS Lett 555: 91-95

22. Colquhoun D, Unwin D, Shelley C, Hatton C, Sivilotti L (2003) In: Abraham D (ed) Burger's Medicinal Chemistry, Vol. 2, Drug Discovery & Drug Development. John Wiley & Sons, New York pp 357-405
23. Grutter T, Le Novere N, Changeux JP (2004) Curr Top Med Chem 4: 645-650
24. Absalom NL, Lewis TM, Schofield PR (2004) Exp Physiol 89: 145-153
25. Doyle DA (2004) Trends Neurosci 27: 298-302
26. Colquhoun D, Sivilotti LG (2004) Trends Neurosci 27: 337-344
27. Lester HA, Dibas MI, Dahan DS, Leite JF, Dougherty DA (2004) Trends Neurosci 27: 329-336
28. Miyazawa A, Fujiyoshi Y, Stowell M, Unwin N (1999) J Mol Biol 288: 765-786
29. Miyazawa A, Fujiyoshi Y, Unwin N (2003) Nature 424: 949-955
30. Brejc K, van Dijk WJ, Klaassen RV, Schuurmans M, van Der Oost J, Smit AB, Sixma TK (2001) Nature 411: 269-276
31. Sixma TK, Smit AB (2003) Annu Rev Biophys Biomol Struct 32: 311-334
32. Smit AB, Brejc K, Syed N, Sixma TK (2003) Ann NY Acad Sci 998: 81-92
33. Celie PH, van Rossum-Fikkert SE, van Dijk WJ, Brejc K, Smit AB, Sixma TK (2004) Neuron 41: 907-914
34. Hibbs RE, Talley TT, Taylor P (2004) J Biol Chem 279: 28483-28491
35. Sine SM (2002) J Neurobiol 53: 431-446
36. Sine SM, Wang HL, Gao F (2004) Curr Med Chem 11: 559-567
37. Dutertre S, Lewis RJ (2004) Eur J Biochem 271: 2327-2334
38. Sine SM, Wang HL, Bren N (2002) J Biol Chem 277: 29210-29223
39. Molles BE, Tsigelny I, Nguyen PD, Gao SX, Sine SM, Taylor P (2002) Biochemistry 41: 7895-7906
40. Sullivan D, Chiara DC, Cohen JB (2002) Mol Pharmacol 61: 463-472
41. Le Novere N, Grutter T, Changeux JP (2002) Proc Natl Acad Sci USA 99: 3210-3215
42. Yassin L, Samson AO, Halevi S, Eshel M, Treinin M (2002) Biochemistry 41: 12329-12335
43. Schapira M, Abagyan R, Totrov M (2002) BMC Struct Biol 2: 1
44. Everhart D, Reiller E, Mirzoian A, McIntosh JM, Malhotra A, Luetje CW (2003) J Pharmacol Exp Ther 306: 664-670
45. Costa V, Nistri A, Cavalli A, Carloni P (2003) Br J Pharmacol 140: 921-931
46. Henchman RH, Wang HL, Sine SM, Taylor P, McCammon JA (2003) Biophys J 85: 3007-3018
47. Espinoza-Fonseca LM (2004) Biochem Biophys Res Commun 320: 587-591
48. Storch A, Schrattenholz A, Cooper JC, Abdel Ghani EM, Gutbrod O, Weber KH, Reinhardt S, Lobron C, Hermsen B, Soskic V, Pereira EFR, Albuquerque EX, Methfessel C, Maelicke A (1995) Eur J Pharmacol 290: 207-219
49. Schrattenholz A, Pereira EF, Roth U, Weber KH, Albuquerque EX, Maelicke A (1996) Mol Pharmacol 49: 1-6
50. Maelicke A, Coban T, Storch A, Schrattenholz A, Pereira EF, Albuquerque EX (1997) J Recept Signal Transduct Res 17: 11-28
51. Lilienfeld S (2002) CNS Drug Rev 8: 159-176
52. Sabey K, Paradiso K, Zhang J, Steinbach JH (1999) Mol Pharmacol 55: 58-66
53. Zwart R, van Kleef RG, Gotti C, Smulders CJ, Vijverberg HP (2000) J Neurochem 75: 2492-2500
54. Arias HR (2000) Neurochem Int 36: 595-645
55. Schrattenholz A, Coban T, Schroder B, Okonjo KO, Kuhlmann J, Pereira EF, Albuquerque EX, Maelicke A (1993) J Recept Res 13: 393-412

56. Schrattenholz A, Godovac-Zimmermann J, Schäfer HJ, Albuquerque EX, Maelicke A (1993) Eur J Biochem 216: 671-677

57. Schroder B, Reinhardt-Maelicke S, Schrattenholz A, McLane KE, Kretschmer A, Conti-Tronconi BM, Maelicke A (1994) J Biol Chem 269: 10407-10416

58. Ewing TJA, Kuntz ID (1997) J Comput Chem 18: 1175-1189

59. Hetényi C, van der Spoel D (2002) Protein Sci 11: 1729-1737

60. Morris GM, Goodsell DS, Halliday RS, Huey R, Hart WE, Belew RK, Olson AJ (1998) J Comput Chem 19: 1639-1662

61. Thompson JD, Gibson TJ, Plewniak F, Jeanmougin F, Higgins DG (1997) Nucleic Acids Res 25: 4876-4882

62. Sali A, Blundell TL (1993) J Mol Biol 234: 779-815

63. Fiser A, Do RK, Sali A (2000) Protein Sci 9: 1753-1773

64. Pettersen EF, Goddard TD, Huang CC, Couch GS, Greenblatt DM, Meng EC, Ferrin TE (2004) J Comput Chem 25: 1605-1612

65. Laskowski RA, MacArthur MW, Moss DS, Thornton JM (1993) J Appl Cryst 26: 283-291

66. Greenblatt HM, Kryger G, Lewis T, Silman I, Sussman JL (1999) FEBS Lett 463: 321-326

67. Canfield DV, Barrick J, Giessen BC (1987) Acta Crystallogr, Sect C: Cryst Struct Commun C43: 977-979

68. Pauling P, Petcher TJ (1973) J Chem Soc, Perkin Trans 2: 1342-1345

69. Sanner MF, Duncan BS, Carrillo CJ, Olson AJ (1999) Pac Symp Biocomput: 401-412

70. Fraczkiewicz R, Braun W (1998) J Comp Chem 19: 319-333

71. SYBYL 7.0, Tripos Inc., 1699 South Hanley Road, St. Louis, Missouri, 63144, USA

72. Smit AB, Syed NI, Schaap D, van Minnen J, Klumperman J, Kits KS, Lodder H, van der Schors RC, van Elk R, Sorgedrager B, Brejc K, Sixma TK, Geraerts WP (2001) Nature 411: 261-268

73. Fiser A, Sanchez R, Melo F, Sali A (2001) In: Watanabe M, Roux B, MacKerell A, Becker O (eds) Computational Biochemistry and Biophysics. Marcel Dekker, New York pp 275-312

74. Cornell WD, Cieplak P, Bayly CI, Gould IR, Merz KM, Jr., Ferguson DM, Spellmeyer DC, Fox T, Caldwell JW, Kollman PA (1995) J Am Chem Soc 117: 5179-5197

75. Carlson BJ, Raftery MA (1993) Biochemistry 32: 7329-7333

76. Schrattenholz A, Roth U, Schuhen A, Schafer HJ, Godovac-Zimmermann J, Albuquerque EX, Maelicke A (1994) J Recept Res 14: 197-208

77. Schrattenholz A, Roth U, Godovac-Zimmermann J, Maelicke A (1997) Biochemistry 36: 13333-13340

78. Chenna R, Sugawara H, Koike T, Lopez R, Gibson TJ, Higgins DG, Thompson JD (2003) Nucleic Acids Res 31: 3497-3500

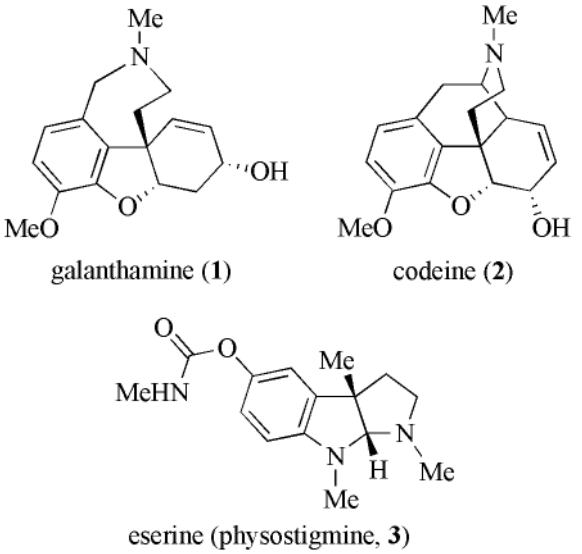

Figure 1 Chemical structures of three allosteric modulators of nicotinic acetylcholine receptors

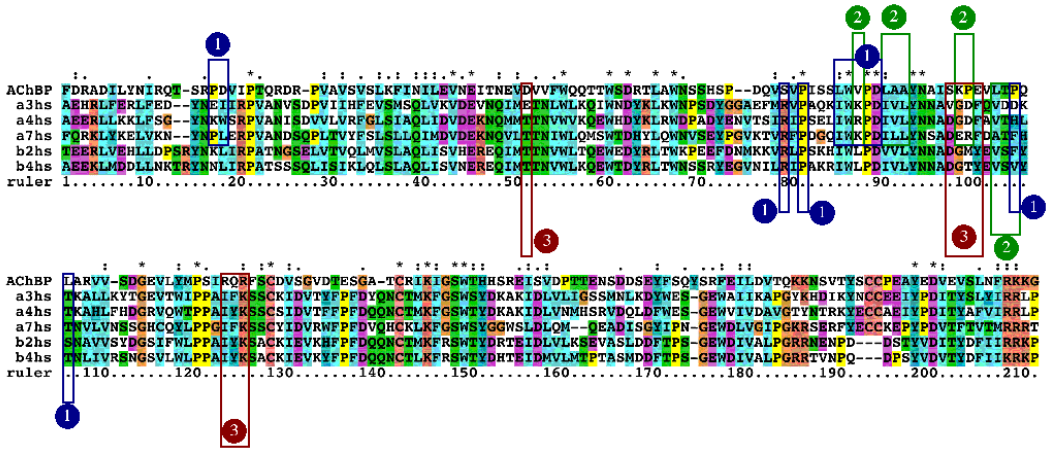

Figure 2 Multiple sequence alignment between AChBP and amino-terminal domains of human α3, α4, α7, β2 and β4 nAChRs subunits, represented with CLUSTALX. [61,78] The stars (*) represent the fully conserved residues, while the dots (:) and (.) represent "strongly" and "weakly" conserved residues, respectively. The boxes represent the most important residues of the three allosteric sites: 1 (blue), 2 (green) and 3 (red). See Tables S1-S3 (Supplementary material) for more detailed information

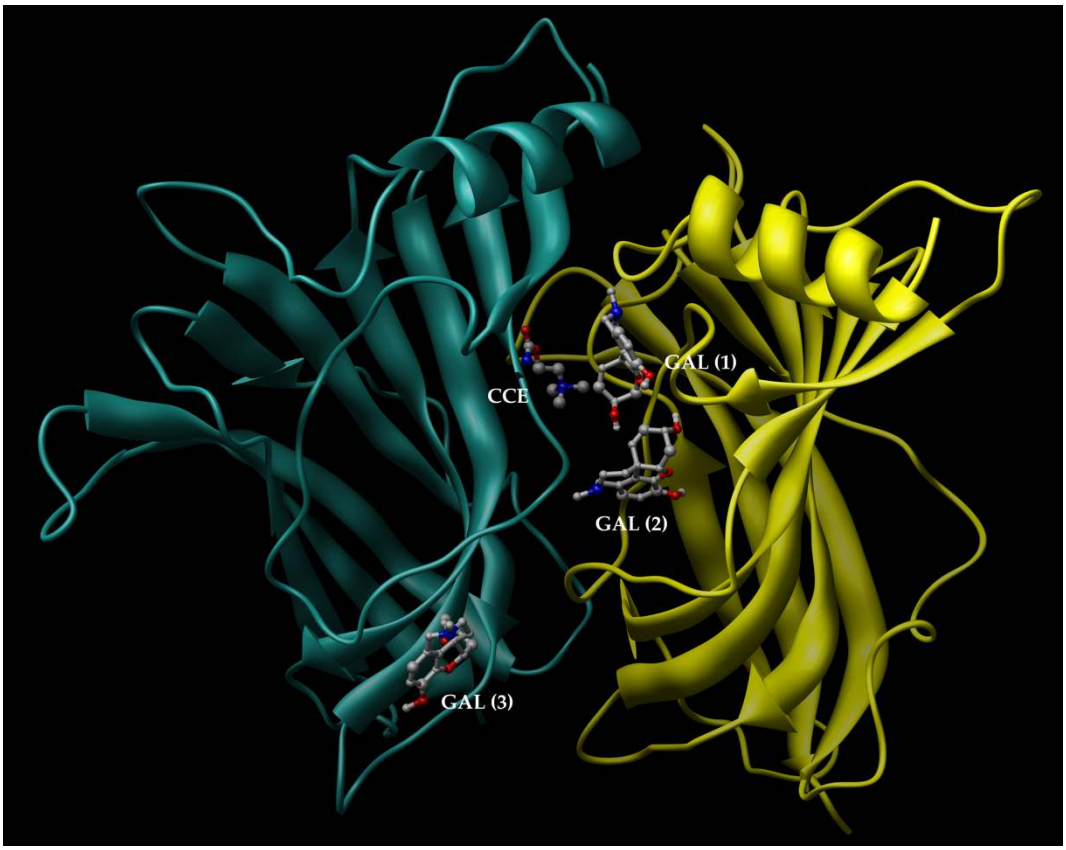

Figure 3. Representation of two subunits of AChBP with carbamoylcholine (CCE) in the agonist binding site (PDB entry code 1UV6, [33] back) and codeine (COD), galanthamine (GAL) and eserine (ESE) in the putative allosteric binding sites (1, 2 and 3, respectively) found using the "blind docking" approach (front)

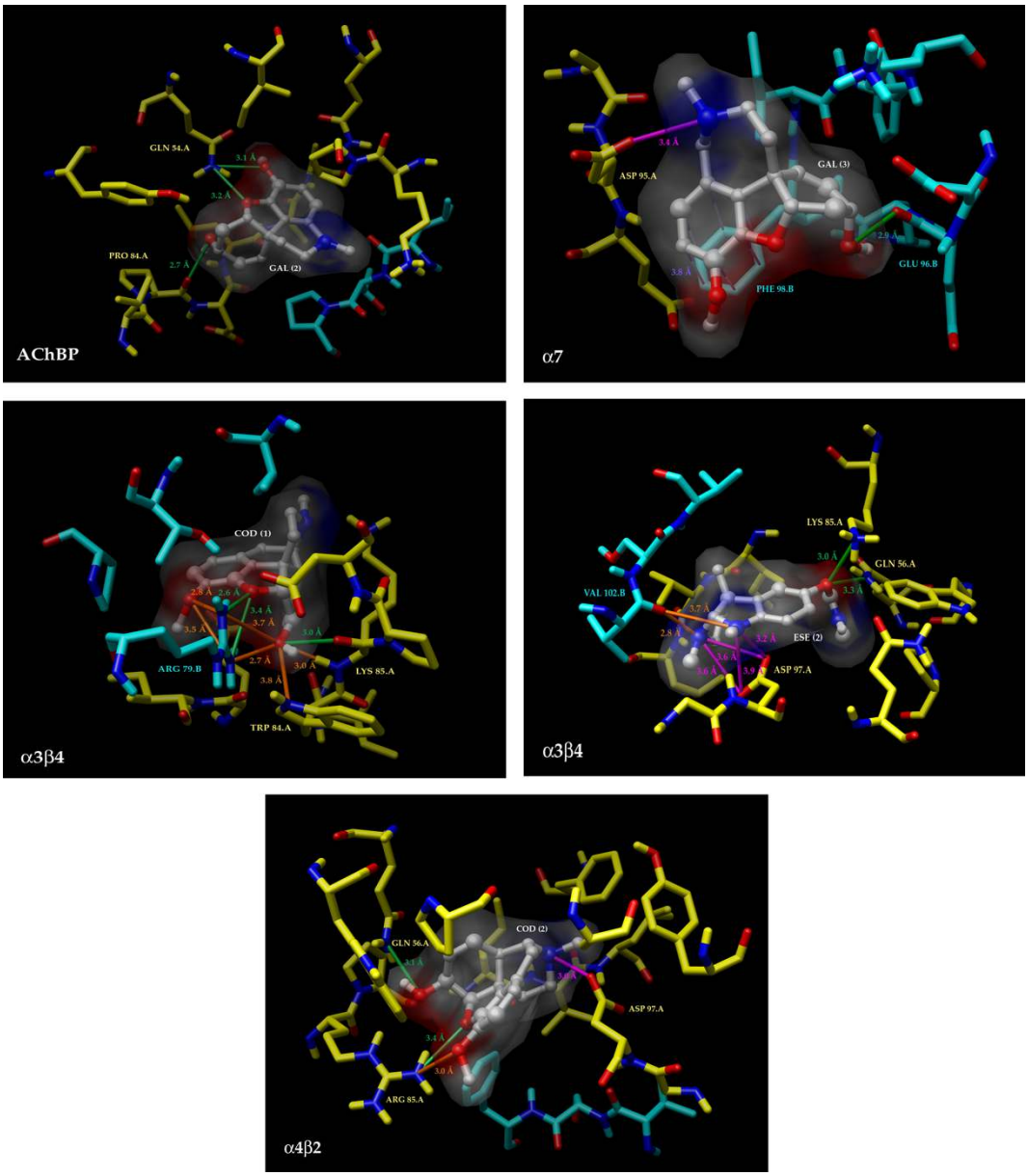

Figure 4 Representative binding modes of the most stable docked orientations of galanthamine with AChBP (site 2), galanthamine with human α7 model (site 3), codeine with human α3β4 model (site 1), eserine with human α3β4 model (site 2) and codeine with human α4β2 model (site 2). See the Supplementary material for several additional examples

Table 1 Percentage of sequence identities computed using MODELLER software [62,63] from the alignment shown in **Figure 2.** The number of identical residues is shown in brackets.

	AChBP	α3hs	α4hs	α7hs	β2hs
α3hs	21.0 (43)				
α4hs	20.5 (42)	61.1 (127)			
α7hs	25.9 (53)	43.2 (89)	44.7 (92)		
β2hs	18.0 (37)	47.8 (99)	52.2 (108)	39.8 (82)	
β4hs	19.5 (40)	47.3 (98)	50.2 (104)	41.7 (86)	70.0 (145)

Supporting Information

Acetylcholine nicotinic receptors: Finding the putative binding site of allosteric modulators using the "blind docking" approach

Bogdan Iorga, Denyse Herlem, Elvina Barré, Catherine Guillou**

Institut de Chimie des Substances Naturelles, CNRS UPR 2301, Av. de la Terrasse, F-91198 Gif sur Yvette, France

Contents :

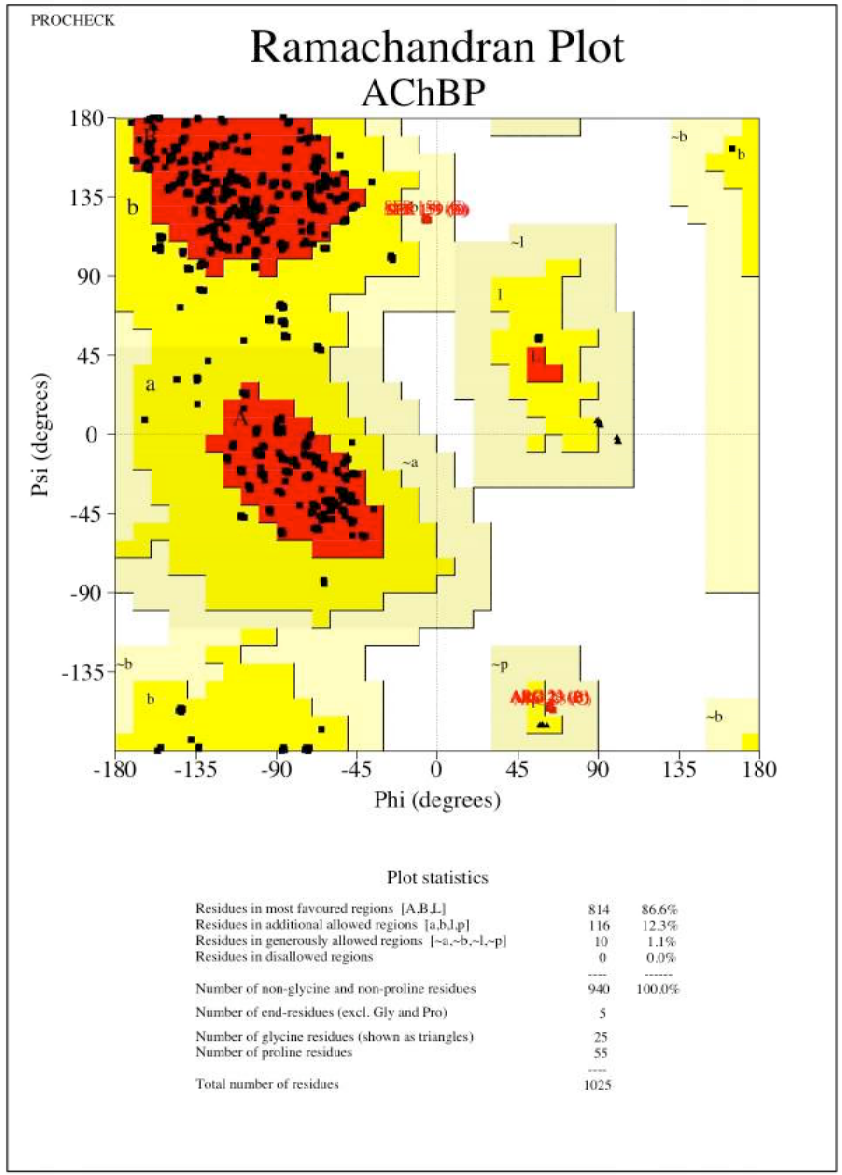
PROCHECK
Ramachandran Plot
AChBP
Psi (degrees)
Phi (degrees)
180
135
90
45
0
-45
-90
-135
-180
-135
-90
-45
0
45
90
135
180
b
a
A
l
L
~b
~l
~a
~p
Plot statistics
Residues in most favoured regions [A,B,L] 814 86.6%
Residues in additional allowed regions [a,b,l,p] 116 12.3%
Residues in generously allowed regions [~a,~b,~l,~p] 10 1.1%
Residues in disallowed regions 0 0.0%
Number of non-glycine and non-proline residues 940 100.0%
Number of end-residues (excl. Gly and Pro) 5
Number of glycine residues (shown as triangles) 25
Number of proline residues 55
Total number of residues 1025

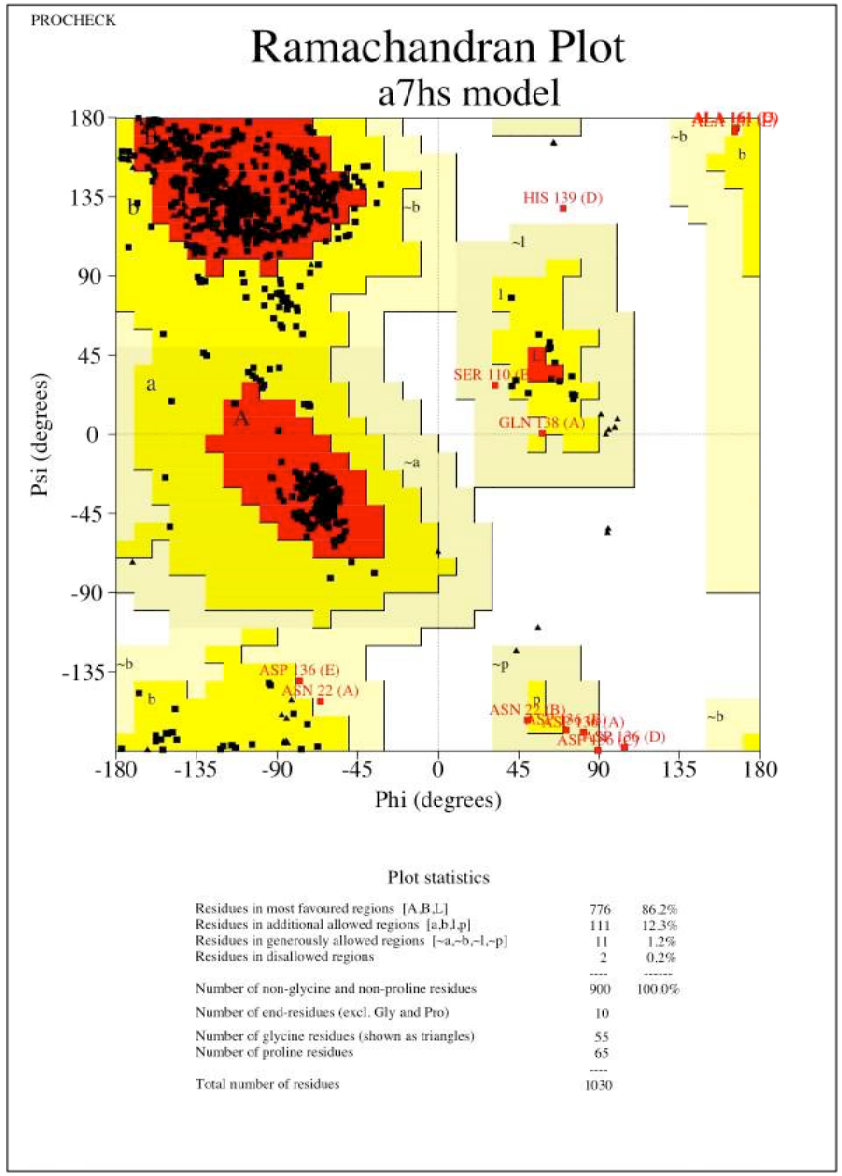
PROCHECK
Ramachandran Plot
a7hs model
Psi (degrees)
Phi (degrees)
HIS 139 (D)
GLN 138 (A)
ASP 136 (E)
ASN 22 (A)
Plot statistics
Residues in most favoured regions [A,B,L] 776 86.2%
Residues in additional allowed regions [a,b,l,p] 111 12.3%
Residues in generously allowed regions [~a,~b,~l,~p] 11 1.2%
Residues in disallowed regions 2 0.2%
Number of non-glycine and non-proline residues 900 100.0%
Number of end-residues (excl. Gly and Pro) 10
Number of glycine residues (shown as triangles) 55
Number of proline residues 65
Total number of residues 1030

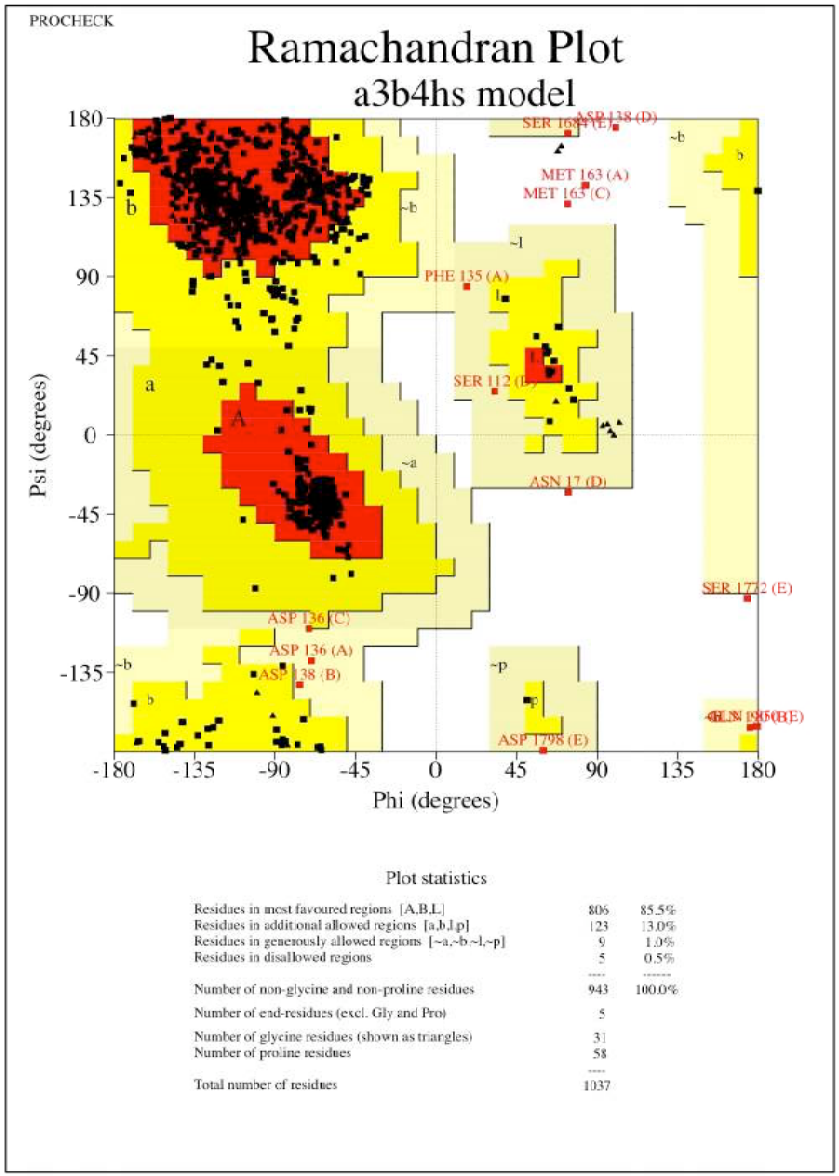
PROCHECK
Ramachandran Plot
a3b4hs model
Psi (degrees)
Phi (degrees)
180
135
90
45
0
-45
-90
-135
-180
MET 163 (A)
MET 165 (C)
PHE 135 (A)
ASN 17 (D)
SER 172 (E)
ASP 136 (C)
ASP 136 (A)
ASP 138 (B)
ASP 179 (E)
Plot statistics
Residues in most favoured regions [A,B,L] 806 85.5%
Residues in additional allowed regions [a,b,l,p] 123 13.0%
Residues in generously allowed regions [~a,~b,~l,~p] 9 1.0%
Residues in disallowed regions 5 0.5%
Number of non-glycine and non-proline residues 943 100.0%
Number of end-residues (excl. Gly and Pro) 5
Number of glycine residues (shown as triangles) 31
Number of proline residues 58
Total number of residues 1037

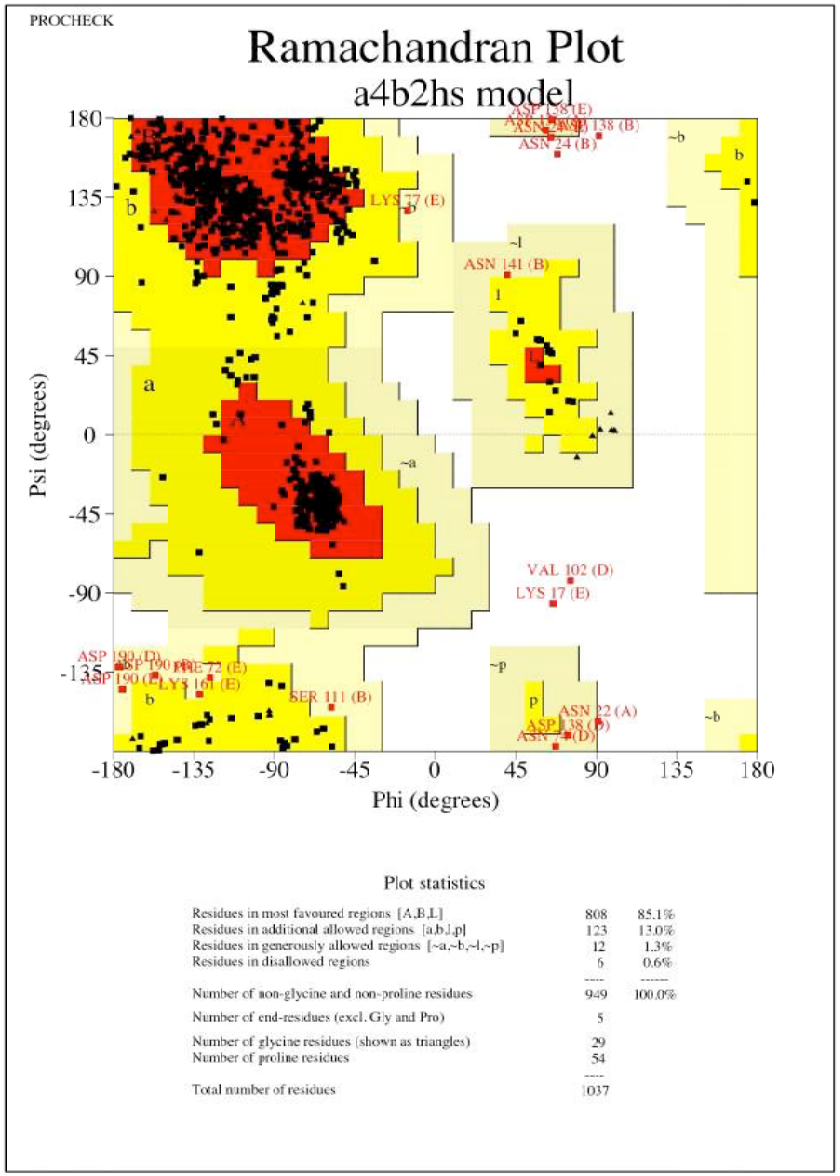
PROCHECK
Ramachandran Plot
a4b2hs model
Psi (degrees)
Phi (degrees)
180
135
90
45
0
-45
-90
-135
-180
LYS 77 (E)
ASN 141 (B)
VAL 102 (D)
LYS 17 (E)
SER 111 (B)
ASN 22 (A)
Plot statistics
Residues in most favoured regions [A,B,L] 808 85.1%
Residues in additional allowed regions [a,b,l,p] 123 13.0%
Residues in generously allowed regions [~a,~b,~l,~p] 12 1.3%
Residues in disallowed regions 6 0.6%
Number of non-glycine and non-proline residues 949 100.0%
Number of end-residues (excl. Gly and Pro) 5
Number of glycine residues (shown as triangles) 29
Number of proline residues 54
Total number of residues 1037

Figure S1. Representative binding modes of the most stable docked orientations of eserine with AChBP (site 1), codeine with AChBP (site 3) and galanthamine with human α7 model (sites 1 and 2). The α/(+) subunits are coloured in yellow and the β/(–) subunits are coloured in blue. The H-bonds are represented in green, the salt bridges in magenta, the ionic interactions in orange and the cation-π or π-π interactions in mauve.

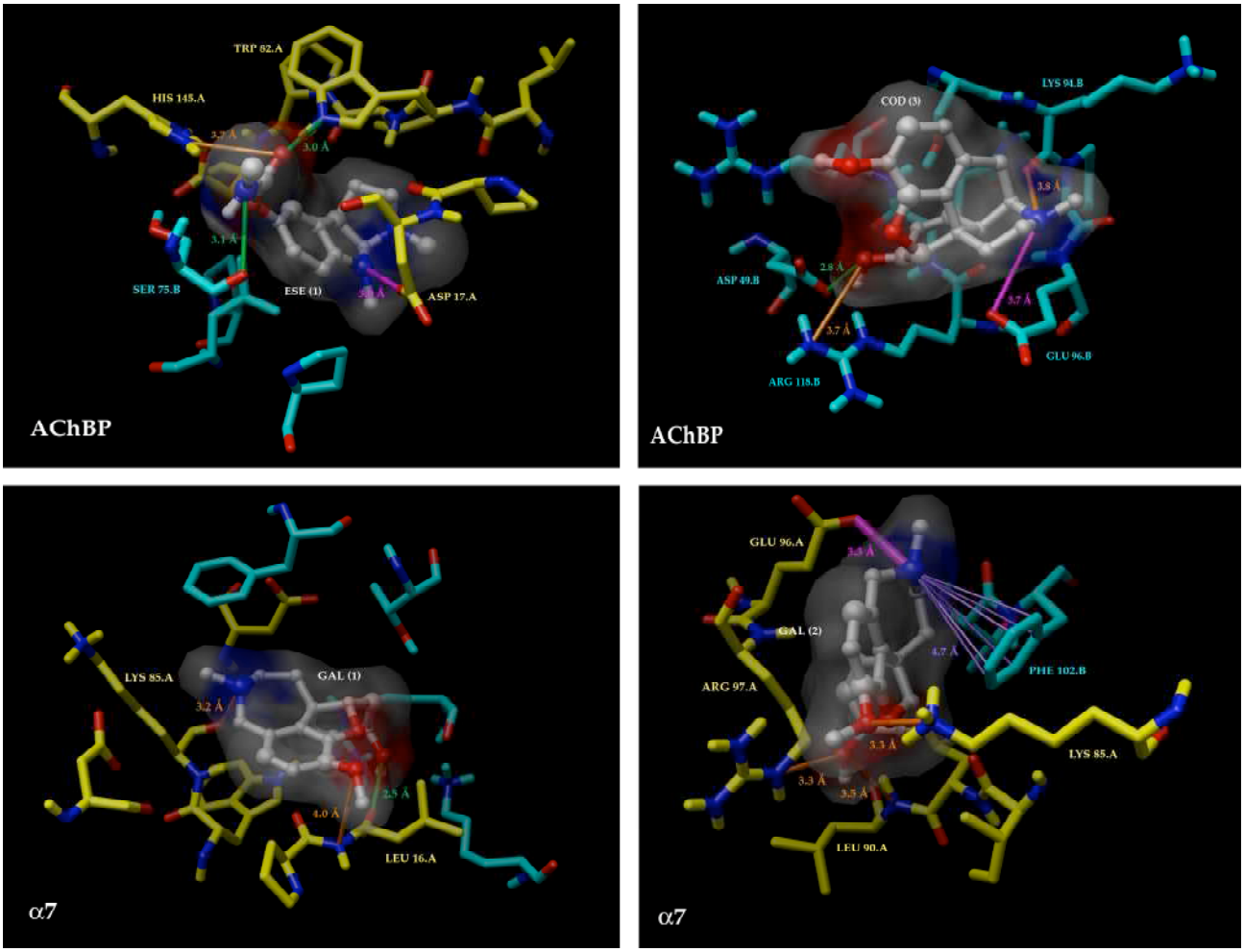

Figure S2. Representative binding modes of the most stable docked orientations of galanthamine with human α3β4 model (sites 1, 2 and 3) and codeine with human α4β2 model (site 1). The α/(+) subunits are coloured in yellow and the β/(–) subunits are coloured in blue. The H-bonds are represented in green, the salt bridges in magenta, the ionic interactions in orange and the cation-π or π-π interactions in mauve.

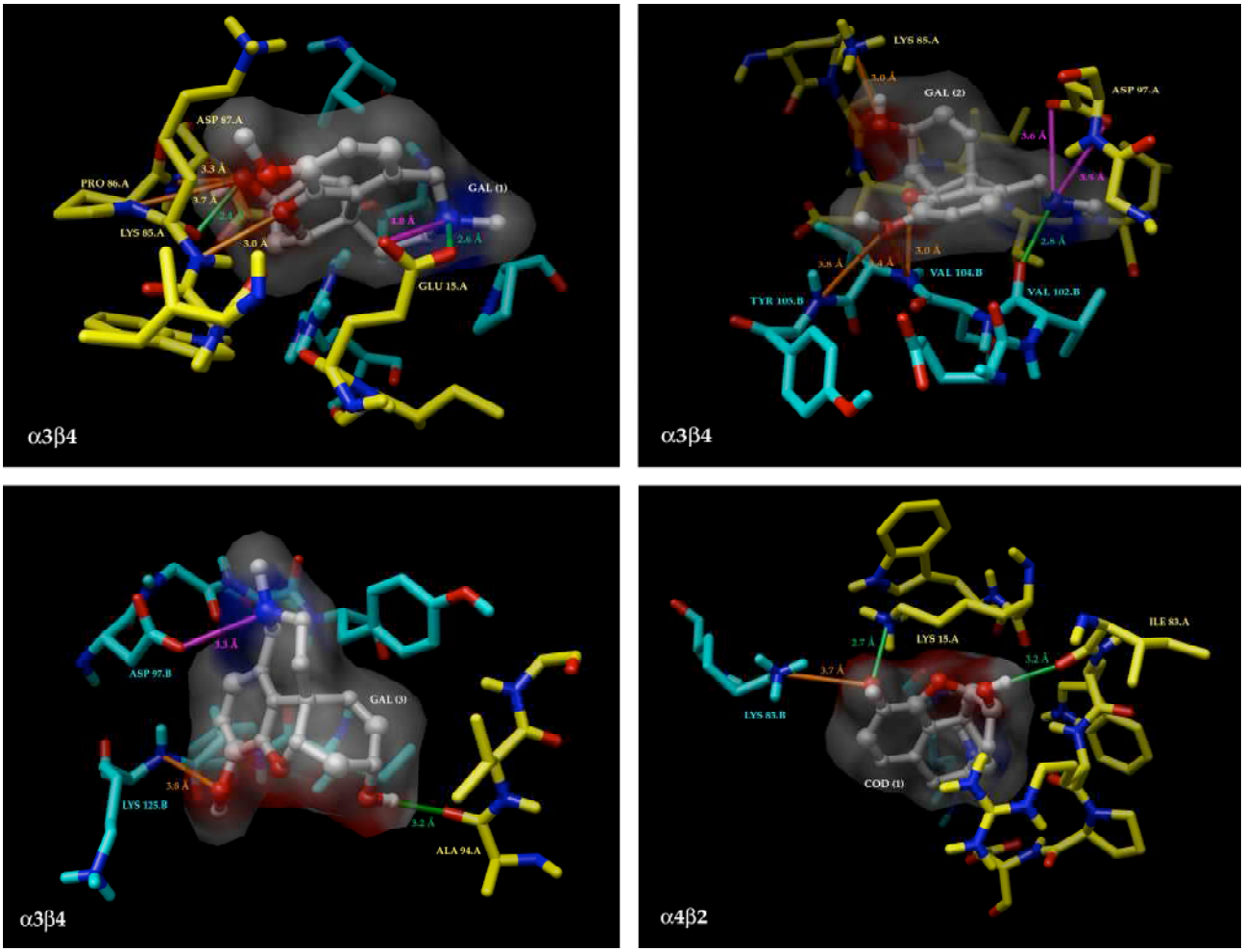

Table S1. Residues in the binding site 1 at less than 5Å from the best docked conformation as found by "refined docking". The conserved positions are coloured in yellow.

aa	AChBP			aa	α7			aa	α3β4			aa	α4 β2		
	COD	ESE	GAL		COD	ESE	GAL		COD	ESE	GAL		COD	ESE	GAL
P16.A	+	+	+	P15.A	+	+	+	E15.A	+	+	+	K15.A	+	+	+
D17.A	+	+	+	L16.A	+	+	+	I16.A	+	+	+	W16.A	+	+	+
V18.A	-	+	+	E17.A	+	+	+					S17.A	-	+	-
I19.A	-	+	+	R18.A	+	+	+					R18.A	-	+	+
I78.A	-	-	+	D80.A	+	+	-	A80.A	+	-	+	S80.A	+	+	+
S79.A	-	-	+	G81.A	-	+	+	Q81.A	+	-	+	E81.A	+	+	+
				Q82.A	-	+	-					L82.A	-	+	-
L81.A	+	+	+	I83.A	+	+	+	I83.A	+	+	+	I83.A	+	+	+
W82.A	+	+	+	W84.A	+	+	+	W84.A	+	+	+	W84.A	+	+	+
V83.A	+	+	+	K85.A	+	+	+	K85.A	+	+	+	R85.A	+	+	+
P84.A	+	+	+	P86.A	+	+	+	P86.A	+	-	+	P86.A	+	+	+
D85.A	+	+	+	D87.A	+	+	+	D87.A	+	-	+	D87.A	+	+	+
L86.A	+	-	+					I88.A	-	-	+				
								K105.A	-	-	+				
T144.A	-	+	-	S148.A	+	+	+					T148.A	+	+	+
H145.A	+	+	+									Y149.A	+	+	+
R3.B	-	+	-												
L7.B	-	+	-	K7.B	+	-	+								
V74.B	-	+	-												
S75.B	-	+	+	R77.B	+	+	+	R79.B	+	+	+	R79.B	+	+	-
V76.B	-	+	-	F78.B	+	+	+					L80.B	-	-	+
P77.B	+	+	+	P79.B	+	+	+	P81.B	+	+	+	P81.B	+	+	+
				D80.B	+	+	-	A82.B	-	+	-	S82.B	-	-	+
								K83.B	-	+	+	K83.B	+	+	+
								R84.B	+	-	+				
P100.B	+	+	+	F102.B	+	+	+	V104.B	+	+	+	F104.B	+	+	+
Q101.B	+	-	+	H103.B	+	+	-	Y105.B	-	+	-	Y105.B	+	+	+
L102.B	+	+	+	T104.B	+	+	+	T106.B	+	+	+	S106.B	+	+	+
R104.B	-	+	-	N105.B	-	+	-	N107.B	-	+	-				

Table S2. Residues in the binding site 2 at less than 5Å from the best docked conformation as found by "refined docking". The conserved positions are coloured in yellow.

aa	AChBP			aa	α7			aa	α3 β4			aa	α4 β2		
	COD	ESE	GAL		COD	ESE	GAL		COD	ESE	GAL		COD	ESE	GAL
				F31.A	+	+	-					F31.A	+	-	-
Q54.A	+	+	+	L54.A	+	+	+	L54.A	+	+	-	V54.A	+	-	+
				M56.A	-	+	-	Q56.A	+	+	-	Q56.A	+	-	-
				D80.A	+	-	-								
V83.A	+	+	+	K85.A	+	+	+	K85.A	+	+	+	R85.A	+	+	-
P84.A	+	+	+					P86.A	+	+	+	P86.A	+	-	-
D85.A	+	+	+					D87.A	+	-	+				
L86.A	+	+	+	I88.A	+	+	+	I88.A	+	+	+	I88.A	+	+	+
A87.A	+	+	+	L89.A	-	+	+	V89.A	+	+	+	V89.A	+	+	+
A88.A	+	+	+	L90.A	-	+	+	L90.A	+	+	+	L90.A	+	+	+
A91.A	+	+	-	S93.A	-	+	+	N93.A	+	+	+	N93.A	-	+	+
S93.A	+	+	-	D95.A	-	+	+	V95.A	+	+	+	D95.A	-	+	+
K94.A	+	+	+	E96.A	+	+	+	G96.A	+	+	+	G96.A	-	+	+
P95.A	+	+	+	R97.A	+	+	+	D97.A	+	+	+	D97.A	+	+	+
				F98.A	+	-	-								
				D99.A	+	+	+	Q99.A	+	+	-	A99.A	+	-	-
				T101.A	+	-	-								
				H103.A	+	+	+					L103.A	+	-	-
Y113.A	+	-	+	Y116.A	+	+	-	W116.A	-	+	-	W116.A	+	-	-
				P118.A	+	+	+	P118.A	-	+	-	P118.A	+	-	-
I117.A	+	+	+									A120.A	+	-	+
Q119.A	+	+	+	F122.A	-	+	+					Y122.A	+	+	+
I140.A	-	-	+	F144.A	+	+	+					F144.A	+	+	-
												Y100.B	-	+	-
V97.B	+	-	+	D99.B	-	+	+	E101.B	+	-	+	E101.B	-	+	+
L98.B	+	+	+	A100.B	-	+	+	V102.B	+	+	+	V102.B	-	+	+
T99.B	+	+	+	T101.B	-	+	+	S103.B	+	+	+	S103.B	-	+	+
P100.B	+	+	+	F102.B	+	+	+	V104.B	+	+	+	F104.B	+	+	+
				H103.B	-	-	+	Y105.B	-	-	+				

Table S3. Residues in the binding site 3 at less than 5Å from the best docked conformation as found by "refined docking". The conserved positions are coloured in yellow.

aa	AChBP			aa	α7			aa	α3 β4			aa	α4 β2		
	COD	ESE	GAL		COD	ESE	GAL		COD	ESE	GAL		COD	ESE	GAL
				A94.A	+	+	+	A94.A	+	-	+	A94.A	-	-	+
				D95.A	+	+	+	V95.A	+	-	+	D95.A	-	+	+
				E96.A	+	+	+	G96.A	+	-	+				
				F98.A	-	-	+								
												K123.A	-	-	+
				M39.B	+	+	+	I41.B	+	+	+	I41.B	-	-	+
E40.B	-	+	-	D40.B	+	-	-	S42.B	+	-	-	S42.B	-	-	+
								M50.B	-	-	+				
D49.B	+	+	+	T49.B	+	+	+	T51.B	+	+	+	T51.B	+	-	+
V50.B	-	+	+					T52.B	+	+	+				
I92.B	-	-	+									A96.B	-	+	-
S93.B	+	+	+	D95.B	+	+	+	D97.B	+	+	+	D97.B	+	+	+
K94.B	+	+	+	E96.B	+	+	+	G98.B	+	+	+	G98.B	+	+	+
P95.B	+	+	-	R97.B	+	+	+	T99.B	-	+	+	M99.B	+	+	+
E96.B	+	+	+	F98.B	+	+	+	Y100.B	+	+	+	Y100.B	+	+	+
V97.B	-	+	-					E101.B	-	+	-				
R118.B	+	+	+	I121.B	+	+	+	I123.B	+	+	+	I123.B	+	+	+
Q119.B	+	+	+	F122.B	+	+	+	Y124.B	+	+	+	Y124.B	+	-	+
R120.B	+	+	+	K123.B	+	+	+	K125.B	+	+	+	K125.B	-	+	+

Table S4. Distribution of populations on the three binding sites and estimated docking energies[#] in "blind docking"

		AChBP			α7			α3 β4			α4 β2		
		COD	ESE	GAL	COD	ESE	GAL	COD	ESE	GAL	COD	ESE	GAL
Population in "blind docking" (%)	Site 1	60.8	61.7	58.3	63.0	34.0	43.6	35.2	16.1	30.7	47.1	21.7	29.6
	Site 2	34.2	23.4	41.0	28.9	55.3	50.6	59.2	78.9	68.1	44.1	58.0	65.6
	Site 3	5.0	14.9	0.7	8.1	10.6	5.8	5.6	5.0	1.2	8.8	20.3	4.8
Mean docking energy in "blind docking" (kcal/mol)	Site 1	-7.8	-6.7	-8.3	-7.8	-6.6	-7.8	-7.9	-7.5	-8.2	-8.6	-6.9	-7.8
	Site 2	-8.1	-6.7	-8.4	-7.5	-6.4	-7.9	-8.1	-6.9	-8.3	-7.4	-6.8	-8.8
	Site 3	-6.9	-6.5	-7.2	-6.6	-5.8	-6.5	-6.8	-5.9	-6.3	-6.6	-6.3	-6.8

Table S5. Estimated docking energies[#] for the best docked conformations in "refined docking"

		AChBP			α7			α3 β4			α4 β2		
		COD	ESE	GAL	COD	ESE	GAL	COD	ESE	GAL	COD	ESE	GAL
Docking energy in "refined docking" (kcal/mol)	Site 1	-9.2	-10.1	-9.4	-9.9	-8.4	-10.2	-8.8	-7.7	-9.3	-12.1	-10.0	-11.5
	Site 2	-9.0	-8.6	-10.0	-9.0	-9.5	-10.7	-9.4	-8.8	-10.2	-10.0	-9.2	-10.6
	Site 3	-8.3	-7.9	-8.5	-8.1	-6.9	-7.6	-7.4	-7.0	-8.0	-7.5	-6.7	-7.6

Table S6. Estimated free binding energies[##] for the best docked conformations in "refined docking"

		AChBP			α7			α3 β4			α4 β2		
		COD	ESE	GAL	COD	ESE	GAL	COD	ESE	GAL	COD	ESE	GAL
Free binding energy in "refined docking" (kcal/mol)	Site 1	-9.0	-9.7	-9.1	-9.7	-8.0	-9.9	-8.6	-7.2	-9.0	-11.8	-9.6	-11.2
	Site 2	-8.8	-8.1	-9.7	-8.8	-9.2	-10.4	-9.3	-8.7	-10.0	-9.8	-8.8	-10.4
	Site 3	-8.0	-7.4	-8.2	-7.9	-6.7	-7.3	-7.3	-6.6	-7.7	-7.2	-6.2	-7.3

[#] Docking energy = Intermolecular energy + Internal energy of the ligand
[##] Free binding energy = Intermolecular energy + Torsional free energy

Table S7. Parameters of the allosteric sites identified by "blind docking" compared with those of the agonist site

Protein	Site	Total area (Å^2)	Polar area (Å^2)	Apolar area (Å^2)	Volume (Å^3)	Depth (Å)
AChBP	1	613	228	385	58	14
	2	481	155	326	28	8
	3	668	254	414	17	5
	agonist	432	115	317	56	10
α7	1	588	169	419	89	8
	2	821	286	535	92	12
	3	858	357	501	27	8
	agonist	328	135	193	40	7
α4β2	1	691	210	481	100	10
	2	679	252	427	89	13
	3	687	214	473	19	8
	agonist	427	143	284	45	8
α3β4	1	780	291	489	56	9
	2	557	237	320	43	10
	3	600	197	403	10	6
	agonist	358	100	258	14	5